의공학회지 : 제15권, 제2호, 1994
J. of KOSOMBE : Vol. 15, No. 2

연 구 논 문
94-15-2-14

Method of Deciding Elastic Modulus of Left and Right Ventricle Reconstructed by Echocardiography Using Finite Element Method and Stress Analysis

Geun-jo Han*, Sang Hyun Kim**

=Abstract=

In order to study the shape and dimensions of heart, a procedure to reconstruct a three dimensional left ventricular geometry from two dimensional echocardiographic images was studied including the coordinate transformation, curve fitting and interpolation utilizing three dimensional position registration arm.

Nonlinear material property of the left ventricular myocardium was obtained by finite element method performed on the reconstructed geometry and by optimization techniques which compared the computer predicted 3D deformation with the experimentally determined deformation. Elastic modulus ranged from 3.5g/cm² at early diastole to 153g/cm² at around end diastole showing slightly nonlinear relationship between the modulus and the pressure.

Afterwards using the obtained nonlinear material propertry the stress distribution related with oxyzen consumption rate was analyzed. The maximum and minimum of σ_1 (max. principal stress) occurred at nodes on the second level intersection points of x-axis with endocardium and with epicardium, respectively. And the tendency of the interventricular septum to be flattened was observed from the compressive σ_1 on the anterior, posterior nodes of left ventricle and from the most significant change of dimension in D_{RL} (septal-lateral dimension of right ventricle).

Key words : Left ventricle, Echocardiographic, Position registration, Nonlinear, Myocardium, Reconstruct, Elastic modulus, Diastole, Stress

INTRODUCTION

A number of attempts have been made to analyze the mechanical behavior of the left ventricle which is closely related with the cardiac performance. Several of these studies have concentrated on the diastolic performance since abnormalities in diastolic function have been suggested to be precursor to systolic dysfunction. The diastolic function is usuallay evaluated by the left ventricular pressure-volume (P-V) curve. Glantz and Kernoff[1] attempted to correlate the coefficients in an exponential P-V relationship assuming the ventricle was a uniform spherical shell. Pinto and Fung[2] also conducted stress-strain testing to investigate the elastic behavior of the heart muscle in the passive state using an exponential equation. But in order to analyse the stress distribution the elastic modulus according to varying pressure should be obtained from the in vivo heart myocardium. The previous studies didn't show the relationship of the elastic modulus with respect to the pressure, E-P curve. Hence our study was focused on the E-P

* Department of Mechanical Engineering, College of Engineering, Dong-A University
** Cardiovascular Research Institute, Yonsei University College of Medicine
통신저자: Geun-jo Han, (604-714) 부산직할시 사하구 하단동 840, Tel. (051) 200-7635, Fax. (051) 200-7656

curve of the in vivo myocardium using the 2D echocardiogram to investigate the stress distribution.

Attempts have also been made to compute the myocardial stress distribution since the underlying myocardial oxyzen demand is colsely related with the level of stress[3~4]. Janz et al[5] studied about the deformation of the diastolic left ventricle using finite element method assuming the inner third and two-thirds of the ventricle wall have Young's modulus of 30 and 60g/cm^2, respectively. McCulloch[6] also studied regional left ventricular epicardial deformation in the passive dog heart experimentally. But these studies analysed only the LV model so that these couldn't explain about the stress affected by the RV and interventricular septum wall motion. To analyse the effect of the RV to the stress distribution and the wall motion, finite element method was employed on the combined model of LV and RV. For these investigations the study of the material properties of the myocardium during passive expansion such as Young's modulus is essential. Finite element technique was used on the three dimensional reconstructed (3D) geometries[7~10] of the left ventricle (LV) to assess the material properties of the myocardium.

In order to determine the nonlinear material[1,2,6,11,12] property of the left ventricular myocardium, a finite element analysis was performed on the reconstructed geometry. The nonlinear analysis was implemented by way of a stepwise linear analysis. The material properties of each step within a diastole were obtained by an optimization technique which compared the computer predicted 3D deformation with the experimentally determined deformation, and the optimized elastic modulus was computed so that an error function representing the total difference might be minimized. These optimized elastic moduli and the pressure increments obtained from the experimental measurements were used to analyse the stress in LV and RV geometry.

ECHOCARDIOGRAPHIC RECORDING

From the pressure recording obtained using calibrated transducer-tipped catheters (Mikrotip #MT-10, Millar Instruments Inc.) inserted into the left and right ventricles via the femoral artery and vein, an interval where discrete pressure increase was observed in diastole was located and divided into three or four small intervals. With the measurement of the pressure increments which would be applied as pressure loads on the reconstructed geometry, the points corresponding to the dividing points in pressure recording were sought on the ECG as time referecne.

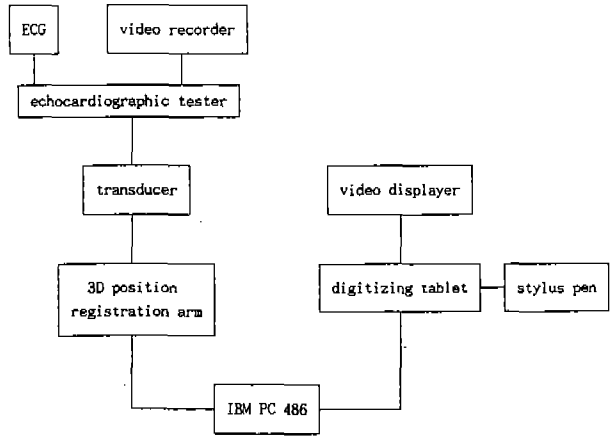

Fig. 1. Schematic diagram of the equipments for the 2D echocardiographic imaging and its position registration.

Cross-sectional echocardiographic images frozen at each dividing points of ECG were traced from the video monitor screen and superposed onto transparent sheets. The schematic diagram for the experiment setup is shown in Fig. 1.

THREE DIMENSIONAL RECONSTRUCTION

3. 1 Digitization of 2D images

The recorded images on the video tape were displayed and frozen in order to trace the endocardial and epicardial borders on transparent papers at various times in diastole. These traced echocardiographic images were digitized by a image processor connected to a computer or a Hewlett-Packard digitizer connected to a Prime computer. In each frame the LV epicardial and endocardial contours were manually traced using the joystick hooked up to the image processor. The 2D LV cross-section image contours were converted to a discrete number of data points which were

denoted by the x and y coordinates on the digitizer local coordinate system.

3. 2 Coordinate transformation

The coordinates of the data points were digitized with respect to the local coordinate axes of the digitizer. In order to get the coordinates of those points with respect to the global coordinate system fixed on the experiment table, the coordinate transformation were performed starting from the digitizer to the table via the transducer and the 3D arm by writing reconstruction program.

3. 3 Nodal points

For the smooth surface of the epicardium and the endocardium reconstructed by this program, curve fitting and interpolation techniques were employed between the digitized points on each SAX (short axis cross section). Therefore some points should be picked up according to the specified total number of the points on each contour. These selected points were refered to as 'nodal points' which were the key points in reconstructing the heart.

3. 4 Curve fittings and interpolation

The process of curve fitting and interpolation on the points were required because SAX's were neither parallel each other nor uniformly spaced and the total number of sections for finite element mesh generation might not always agree with the actual number of input SAX.

It was performed on the nodal points lying on the same long axis cross-section (LAX), i. e. the intersections of the contours and the same circular grid on each SAX.

OPTIMIZATION

The execution of the finite element analysis yielded the displacements of each nodes as well as the stress and strain of each element and reaction forces on the constrained nodes. The deformed geometry predicted by the FEM were compared with the reconstructed geometry from the echocardiographic images at the next time point, and modified by the optimized elastic modulus to have the two geometries match as closely as possible. Therefore there may be various ways of comparison and reduction of the mismatch. For most cases, the difference between the calculated displacements and the experimentally obtained displacements of each nodal points had to be utilized. In optimization algorithm 1, object function E_1 as below should be minimized. And E_2 should be minimized in algorithm 2.

$$E_1 = \sum_{i=1}^{n} \{[(x_{Li} - x_{Ei})^2 + (y_{Li}-y_{Ei})^2 + (z_{Li} - z_{Ei})^2]^{2/3} - \alpha(d_{ci}^{x^2} + d_{ci}^{y^2} + d_{ci}^{z^2})^{1/2}\}^2 \quad (4.1)$$

$$E_2 = \sum_{i=1}^{n} \{[(x_{Li} - x_{Ei})^2 + (y_{Li}-y_{Ei})^2 + (z_{Li} - z_{Ei})^2]^{1/2} - \alpha(d_{ci}^{x^2} + d_{ci}^{y^2} + d_{ci}^{z^2})^{1/2}\} \quad (4.2)$$

where n is the number of the considered nodal points and d_{ci}^{x} , X_{Li}, and X_{Ei} are the calculated displacement and x coordinates of the node in the reconstructed geometry in early and late diastole, respectively. d_{ci}^{y} , y_{Li}, y_{Ei}, d_{ci}^{z} , z_{Li}, z_{Ei} denotes the same.

RESULTS AND DISCUSSION

Results of four experiments were plotted together in Fig. 2 and Fig. 3 with the pressure difference as applied loads as shown in Table 1. They were also obtained in two optimization algorithms and compared. The displacement of endocardium were regarded to be more important since it showed a remarkable change whereas epicardium showed little change which was believed due to the pericardium constraining the movement of epicardium as observed in the echocardiac images.

When the geometric nonlinearity was included, the elastic modulus ranged from 3400 dyne/cm^2 (3.5g/cm^2) at early diastole to 150000 dyne/cm^2 (153g/cm^2) at around end diastole. The slope of the best fitting lines for the E-P plottings varied from 28.2 when the endocardium and the optimization algorithm 2 were used, to 41.6 when both contours and the optimization algorithm 1 were used.

From the experiments, the length of long, short axis and longitudinal axis were obtained and standardized to construct ellipsoid with major axis of 65 mm, minor axis of 48. 75 mm and longitudinal axis of 55 mm. The left ventricular myocardial thickness along the major axis was 12 mm and

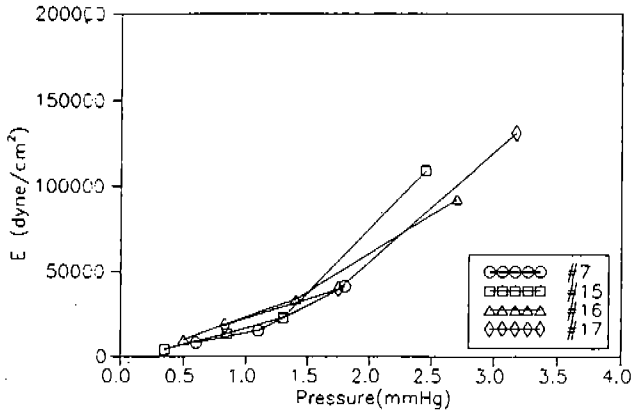

Fig. 2. Comparison of E-P curves of each experiment using optimization algorithm 1 and only endocardium

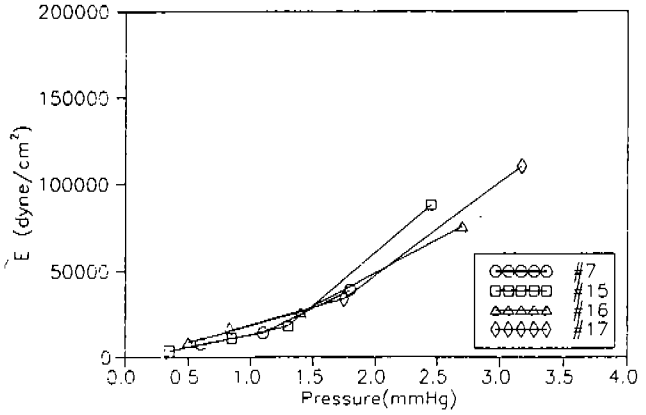

Fig. 3. Comparison of E-P curves of each experiment using optimization algorithm 2 and only endocardium

the right ventricular thickness was 6 mm.

To investigate the effect of nonlinear material property with the stepwise linear technique, we selected 9 loading cases. For the loading cases #1 to #5, an incremental pressure, 0.2mmHg obtained by dividing 1mmHg with 5 increments was applied and 5 different Young's moduli, 220 dyne/mm², 260 dyne/mm², 300 dyne/mm², 340 dyne/mm², 380 dyne/mm² were used, whose values were obtained from the E-P curve connecting two points (200 dyne/mm² at 1 mmHg) and (400 dyne/mm² at 1 mmHg) and dividing that line into 5 intervals. The mean values of Young's modulus for each interval were picked. In #6 and #7 cases, 1 mmHg was applied as a load and 200 dyne/mm², the starting value and 300 dyne/mm², the mean value between 200 dyne/mm² and 400 dyne/mm² were used as Young's modulus on the combined geometry of LV and RV. In #8 and #9 cases, all conditions were same exept that the simulation was implemented on LV geometry alone in order to understand the effect of RV geometry to LV.

Table 1. LV pressures and increments measured at several moments between early and late diastole.

Experiment	P_0	δP_1	P_1	δP_2	P_2	δP_3	P_3	δP_4	P_4
				(mmHg)					
#7	0.20	0.60	0.80	0.50	1.30	0.70	2.00		
#15	3.70	0.35	4.05	0.50	4.55	0.45	5.00	1.15	6.15
#16	3.90	0.50	4.40	0.90	5.30	1.30	6.60		
#17	1.42	0.83	2.25	0.92	3.17	1.42	4.58		

When only the left ventricle model was analysed, its maximum principal stress (σ_1) decreased along the endocardium from 0° to 90° in the counter-clockwise direction as shown in Fig. 4. It also decreased when plotted as in Fig. 6 from the top level to the bottom except that the stress curve for the top level was lower than those for the next two levels. It might result from the fact that the top level of the myocardium was cut through and open in the model even though the real ventricle should be closed and connected with atria. Hence, if the model was constructed so as to represent a whole heart composed of left and right ventricles as well as left and right artia the top level with largest dimensions compared with lower levels might have shown the highest stress distribution.

In other words, the deformation of the upper level above the top level, if the 4 chambers were modeled, would give bending effect to the top level. These trends were also found in the combined model of LV and RV as shown in Fig. 5(a)-(b), Fig. 7. But the magnitude of σ_1 for the combined geometry was quite larger than those of the LV model, because the interventricular septum was affected by RV pressure as well as LV pressure. Lateral side of left ventricular endocardium showed slightly lower σ_1 distribution than the septal side of left ventricular endocardium in LV model. And the stress on the septal side of left ventricular epicardium of combined model on level #1~#4 was compressive but the absolute value of those decreased from the node of

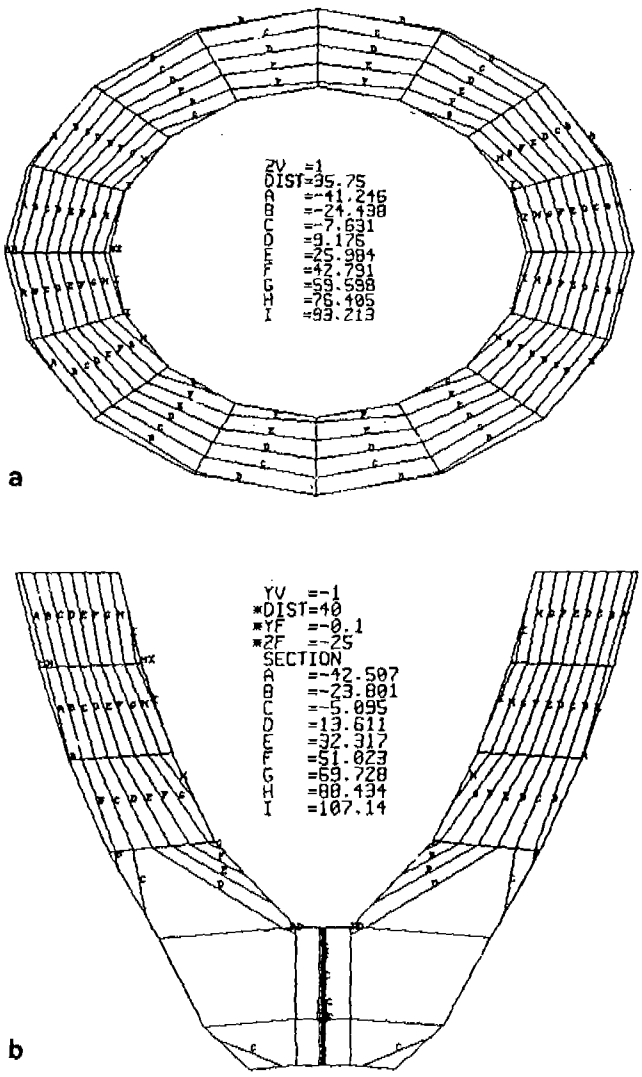

Fig. 4.(a) σ_1 distribution on top level of left ventricle model
(b) σ_1 distribution on the middle section of left ventricle model cut along x-axis

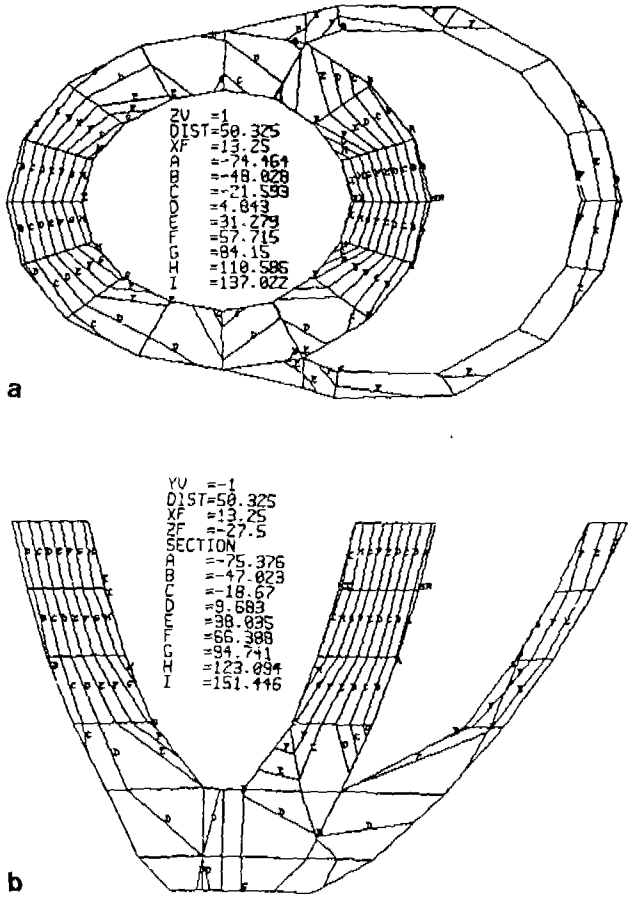

Fig. 5.(a) σ_1 distribution on top level of combined model
(b) σ_1 distribution on the middle section of combined model cut along x-axis

$\theta = 0°$ to the node of $\theta = 45°$ as shown in Fig. 8. Fig. 4(b), 5(b), 6, 7 showed the max. value of σ_1 occurred on the node of second level endocardium with $\theta = 0°$ and the min. value of σ_1 occurred on the node of same level epicardium with same θ.

In case of #1 to #5 of stepwise linear study, the same incremental pressure 0.2 mmHg was applied on the geometry which was deformed geometry of previous stage. For example, in case #3, 0.2 mmHg was applied inside the LV and RV whose initial combined geometry was the deformed one of #2 case. Hence, the coordinates of nodes in the initial geometry were obtained by adding those of initial geometry and the displacements of #2 case.

We could observe that displacement of RV was quite larger than that of LV because the right ventricular wall thickness was thinner than LV thickness and that elliptical shape turned into round shape with almost same length of x and y axis in both LV and RV as shown in Fig. 9 (a)~(b).

According to Fig. 10 where the displacement was plotted based on the previous deformed shapes, D_{AP} (Anterior-posterior dimension) change of case #5 in absolute value was 4.8 times larger than D_{SL} (Septal-lateral dimension for LV) change. The most significant change was observed in D_{RL} (Septal-lateral dimension for RV) because RV was de-

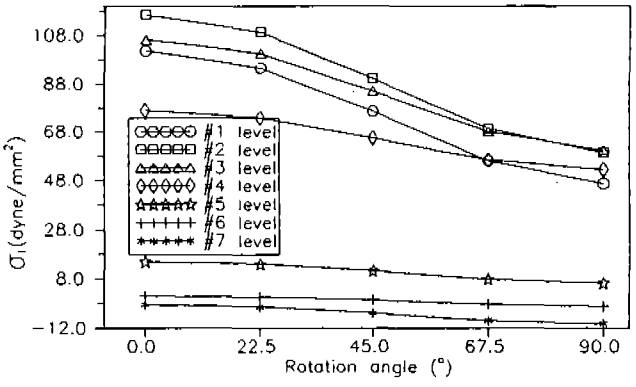

Fig. 6. Change of σ_1 depending on rotation angle θ on endocardium for 7 short axis levels of LV model

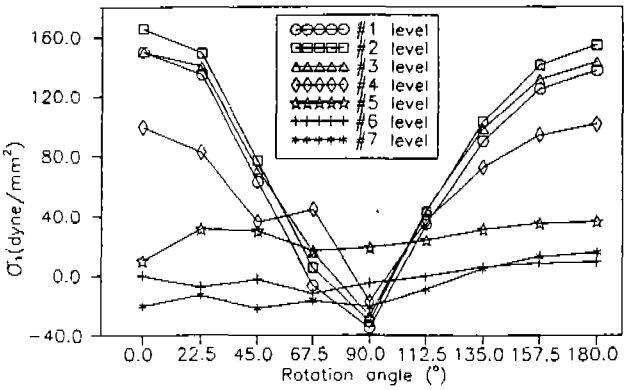

Fig. 7. Change of σ_1 depending on rotation angle on endocardium for 7 short axis levels of combined model

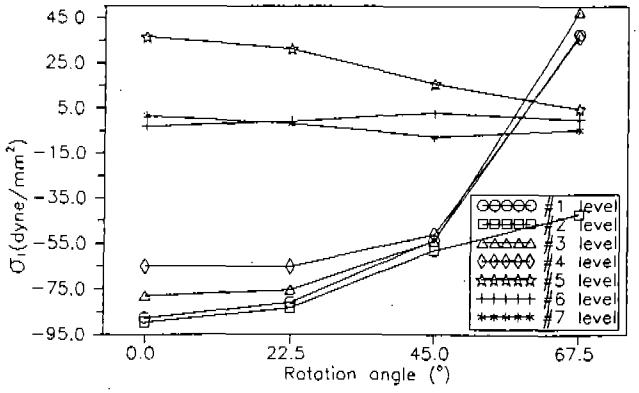

Fig. 8. Change of 1 depending on rotation angle on epicardium for 7 short axis levels of combined model

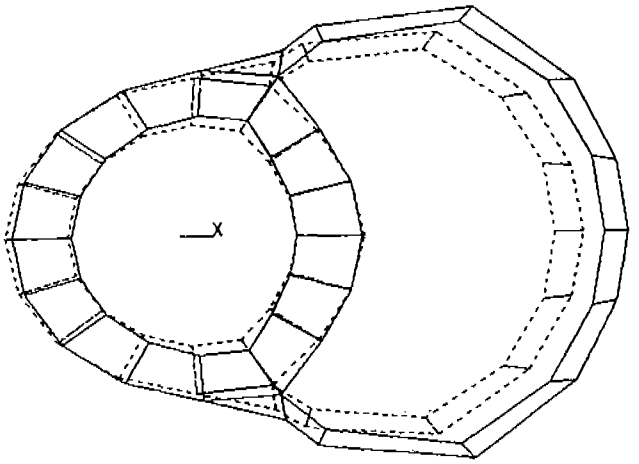

Fig. 9.(a) Deformed shape (solid line) with initial geometry (dashed line) of top level for case # 5

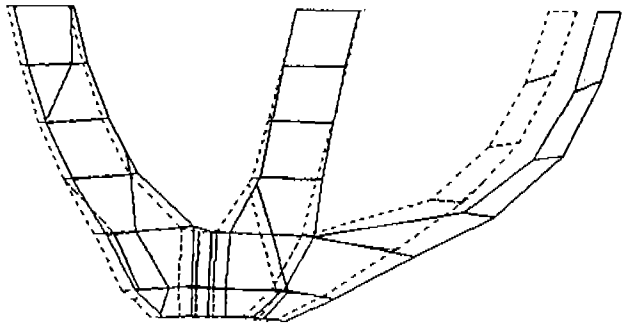

Fig. 9.(b) Deformed shape (solid line) with initial geometry of middle section cut along x-axis for case # 5

formed a lot more due to comparatively thin wall. In case of #5 analysis D_{RL} change was 2.7 times larger than D_{AP} change. All the dimensional change in absolute value increased from case #1 to #5 because the initial geometry got bigger although the applied load was same.

Comparing case #5 where 380 dyne/mm² and 0.2 mmHg were used for Young's modulus and pressure load and case #6 where 200 dyne/mm² and 1 mmHg were used for the same parameters, we might expect that case #6 would bring out bigger displacement than case #5 because of the softer material property and higher pressure of case #6. But the result was reverse. From this fact we could conclude that the initial geometry size exhibited more significant effect on the displacement than Young's modulus and

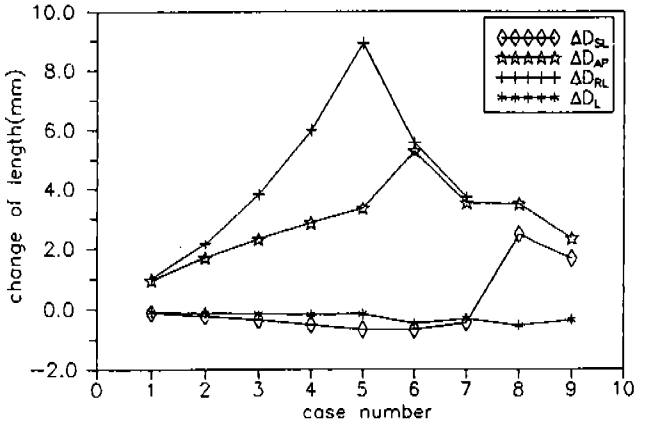

Fig. 10. Change of dimensions for 9 cases

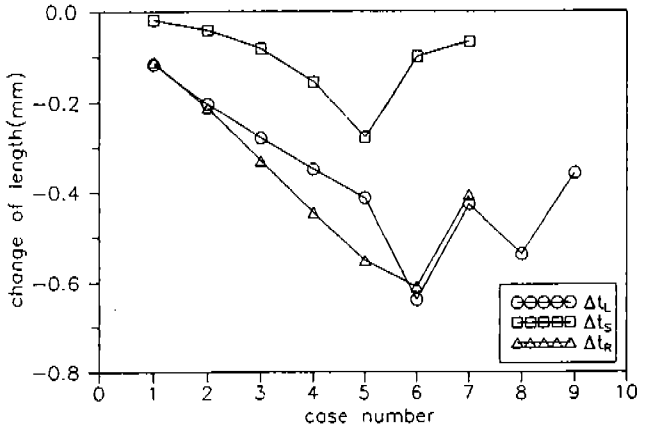

Fig. 11. Change of thickness for 9 cases

ventricular pressure.

We could observe the flattening tendency of septum in the combined geometry of LV and RV whereas the geometry of LV expanded sustaining almost the same eccentricity. So D_{SL} change increased in LV model and decreased in combined model. D_{AP} change increased in both models but D_{AP} of combined model changed more than that of LV model. Little difference in change of D_L (Longitudinal dimension) was found in 2 models, which meant RV geometry gave little effect in D_L change.

The largest thickness change occurred in t_R as shown in Fig. 11. Next were t_L, t_S, successively, that were right ventricular wall thickness, left ventricular wall thickness, and septal thickness, respectively. It could also be found that ts change in LV model was larger than that in the combined model because the LV model expanded freely but the combined model couldn't expand as freely as LV model due to RV geometry and RV pressure. But t_L change was larger in combined model because LV lateral side could expand freely which meant the lateral side of LV in combined model expanded more whereas the septum of LV expanded less than those of LV model.

CONCLUSIONS

The three dimensional reconstruction technique from the two dimensional echocardiographic images and the optimization algorithms in order to investigate the changing trend of elastic modulus depending on the ventricular pressure were described. With the obtained nonlinear material property, stress distribution on the simulated geometry of LV and RV was implemented.

From the experiments and simulation following conclusions were obtained

1. When the geometric nonlinearity was included, the elastic modulus ranged from 3400 dyne/cm^2 (3.5g/cm^2) at early diastole to 150000 dyne/cm^2 (153g/cm^2) at around end diastole.
2. The maximum and minimum of σ_1 in total geometry occured at nodes on the second level, intersection points of x-axis with endocardium and with epicardium, respectively.
3. Lower level exhibited lower σ_1 distribution except the top level which brought about the need for modeling the whole heart with two ventricles and two atria.
4. Node on anterior or posterior showed minimum σ_1 along endocardium on a same level which was tensile in LV model and compressive in combined model because interventricular septum had the tendency to be flattened.
5. The most significant change of dimension in D_{RL}, which led to the same change in t_R, and shrinkage of D_{SL} resulted in the leftward shift of septum.

ACKNOWLEDGEMENT

This paper is part of the research performed by the support of nondirected research fund, Korea Research Foundation, 1992. The author wish to appreciate everyone concerned with KRF.

References

1. S. A. Glantz, R. S. Kernoff, Muscle stiffness determined from canine left ventricular pressre-volume curves, Circ. Research, 37:787-794, 1975
2. J. G. Pinto, Y. C. Fung, Mechanical properties of the heart muscle in the passive state, J. Biomechanics, 6:597-616, 1973
3. R. Beyar, and S. Sideman, Left ventricular mechanics related to the local distribution of oxygen demand throughout the wall, Circ. Res., 58, 664-677, 1986
4. I. Mirsky, D. N. Ghista, H. Sandler, Cardiac Mechanics: Physiological, clinical, and mathematical considerations, John Wiley & Sons Inc., New York, 1974
5. R. F. Janz and A. F. Grimm, Deformation of the diastolic left ventricle, Biophysical J., 13:689-704, 1973
6. A. D. McCulloch, B. H. Smaill, and P. J. Hunter, Regional left ventricular epicardial deformation in the passive dog heart, Circ. Res., 64, 721, 1989.
7. E. A. Geiser, D. J. Skorton, and D. A. Conetta, Quantification of left ventricular function from two-dimensional echocardiography, Am. J. Heart, 103, 903-910, 1982.
8. K. R. Stickels, Wann, L. S An analysis of three-dimensional reconstructive echocardiography, Ultrasound in Med. & Biol., 10, 575-580. 1984.
9. G. Joskowicz, M. Klicpera, P. Pachinger, Computer supported measurements of 2-D echocardiographic images, 1981 Computers in Cardiology, IEEE Computer Society, 13, 1981
10. H. Sawada, J. Fujii, K. Kato, M. Onoe, Y. Kuno, Three dimensional reconstruction of the left ventricle from multiple cross sectional echocardiograms, Br. Heart J., 50:438, 1983
11. J. D. Humphrey, R. K. Strumpf, and, F. C. P. Yin, Determination of a constitutive relation for passive myocardium: I. A new functional form, ASME J. of Biomechanical Engineering, 112, 333, 1990
12. L. A. Taber, On a nonlinear theory for muscle shells: II. Application to the active left ventricle, ASME J. of Biomechanical Engineering, 113, 63, 1991.

=국문초록=

심장의 확장기 특성은 수축기 기능을 파악하기 위한 중요한 자료로 사용될 수 있으므로 압력에 따른 심근의 기계적 탄성 계수의 변화가 유한 요소법을 이용하여 연구되었다. 이를 위하여 2차원 echocardiographic image를 사용하여 심실의 3차원 형상을 재구성 하였는데 3차원 위치 측정 장치로 부터 얻어진 2차원 영상의 상대 위치 각도를 구하여 작성된 프로그램으로 디지타이저 좌표계로 부터 공간 고정 좌표계로 변환하고 다시 국부 좌표계로 변환하며 curve fitting, interpolation 등의 과정을 수행하였다. 압력 변환기로 부터 기록된 좌심실과 우심실내 확장 초기와 확장 말기 사이의 압력차를 여러 단계로 나눠 작용시켜 유한 요소법을 사용하여 각 절점들의 변위를 구하였다. 좌심실 심근의 비선형 재료 특성을 구하기 위하여 다단계 선형 해석을 하였고 확장기내 각 단계에서의 재료 특성은 심외막, 심내막의 측정된 변위와 유한 요소법으로 계산된 변위와의 차를 최소화 시키는 방법으로 구하였다. 측정된 각 단계에서의 압력과 최적화된 탄성 계수로 탄성 계수-압력선도를 그렸고 이 관계를 좌, 우심실이 조합된 모델에 유한 요소법으로 적용시켜 나타나는 변위와 응력 분포를 구하여 이완기 초기와 말기 사이에 탄성 계수가 3.5g/cm²에서 153g/cm²으로 약간의 비선형을 보이면서 증가함을 알았고 우심실의 압력으로 심실 중격이 펴질려는 경향이 있다는 것을 좌심실의 전, 후 절점에서의 압축 σ_1 (최대 주응력)과 D_{RL}(심실 중격과 우심실 자유 측면 사이의 거리)의 증가로 알 수 있었다.